A&A 448, 579–588 (2006)
DOI: 10.1051/0004-6361:20054113

Astronomy & Astrophysics

The GSC-II-based survey of ancient cool white dwarfs⋆,⋆⋆,⋆⋆⋆

I. The sample of spectroscopically confirmed white dwarfs

D. Carollo[1], B. Bucciarelli[1], S. T. Hodgkin[3], M. G. Lattanzi[1], B. McLean[2], R. Morbidelli[1], R. L. Smart[1], A. Spagna[1], and L. Terranegra[4]

[1] INAF – Osservatorio Astronomico di Torino, 10025 Pino Torinese, Italy
e-mail: carollo@to.astro.it
[2] Space Telescope Science Institute, 3700 San Martin Drive Baltimore, MD 21218, USA
[3] Cambridge Astronomical Survey Unit, Institute of Astronomy, Madingley Road,Cambridge, CB3 0HA, UK
[4] INAF – Osservatorio Astronomico di Capodimonte, via Moiariello 16, 80131 Napoli, Italy

Received 27 August 2005 / Accepted 2 November 2005

ABSTRACT

The GSC-II white dwarf survey was designed to identify faint and high proper motion objects, which we used to define a new and independent sample of cool white dwarfs. With this survey we aim to derive new constraints on the halo white dwarf space density. Also, these data can provide information on the age of thick disk and halo through the analysis of the luminosity function. On the basis of astrometric and photometric parameters, we selected candidates with $\mu \gtrsim 0.28''$ yr^{-1} and $R_F \gtrsim 16$ in an area of 1150 square degrees. Then, we separated white dwarfs from late type dwarfs and subdwarfs by means of the reduced proper motion diagram. Finally, spectroscopic follow-up observations were carried out to confirm the white dwarf nature of the selected candidates. We found 41 white dwarfs of which 24 are new discoveries. Here we present the full sample and for each object provide positions, absolute proper motions, photometry, and spectroscopy.

Key words. stars: white dwarfs – astrometry – techniques: spectroscopic – surveys

1. Introduction

Understanding the nature of the Baryonic Dark Matter in the galactic halo is a very fundamental subject of astrophysics. The most favoured candidates are brown dwarfs, planets, ancient cool white dwarfs (WDs), neutron stars and primordial black holes. All these objects are known as MACHOs (Massive Compact Halo Objects) and, in principle, could be detected by their gravitational microlensing effect on field stars (Pacynski 1986). The two major experiments for the detection of microlensing events are MACHO (Alcock et al. 2000) and EROS (Afonso et al. 2003). They measured several events toward the Galactic bulge and the Large (LMC) and Small Magellanic Clouds (SMC). The excess of events towards the Magellanic Clouds is directly related to the dark matter in the halo of our Galaxy, and their interpretation is still under discussion. One potential explanation for these events is that the lenses belong to the halo and, in this case, the MACHO experiment seems to indicate that ∼20% of the dark halo is made of compact objects with mass of 0.5 $M_\odot$ (Alcock et al. 2000). At the moment this evaluation of the baryonic content of the dark halo is controversial because, recently, the EROS-2 collaboration claimed a new value of ∼3%, using a refined set of data (Tisserand & Milsztajn 2005). Moreover, new photometric measures of the microlensing event MACHO-LMC-5 confirmed that the lens is an M 5 dwarf star of 0.2 $M_\odot$ and could suggest another explanation for the microlensing events, i.e. the lenses belong to a previously undetected component of the disk of the Milky Way (Nguyen et al. 2004). If the lenses belong to the halo, the natural candidates that explain the MACHOs and EROS results are very old cool WDs with a mean mass around 0.5 $M_\odot$, and several surveys have been carried out in order to detect a significant number of Population II WDs (see the review by Hansen & Liebert 2003 and Reid 2005).

⋆ Based on observations made with the Italian Telescopio Nazionale Galileo (TNG) operated on the island of La Palma by the Centro Galileo Galilei of the INAF (Istituto Nazionale di Astrofisica) at the Spanish Observatorio del Roque de los Muchachos of the Instituto de Astrofisica de Canarias.

⋆⋆ Based on observations made with the William Herschel Telescope and Isaac Newton Telescope operated on the island of La Palma by the Isaac Newton Group in the Spanish Observatorio del Roque de los Muchachos of the Instituto de Astrofisica de Canarias.

⋆⋆⋆ Tables 2–4 are available in electronic form at the CDS via anonymous ftp to cdsarc.u-strasbg.fr (130.79.128.5) or via http://cdsweb.u-strasbg.fr/cgi-bin/qcat?J/A+A/448/579 and at http://www.edpsciences.org

Here we present a new survey based on the material used for the construction of the GSC-II (Guide Star Catalogue II) (McLean et al. 2000). This survey was developed in order to search for faint and high proper motion objects and to define a new sample of cool WDs. This paper presents the catalogue of the spectroscopically confirmed WDs. Section 2 describes the GSC-II material, astrometry, photometry, and proper motions. In Sect. 3 we present the selection criteria for the candidates, while in Sect. 4 we give details of the spectroscopic observations. Finally in Sect. 5 we describe the WD sample and discuss some interesting objects.

2. The GSC-II plate material and processing

The Guide Star Catalog II is an all-sky database based on the photographic surveys carried out with the Schmidt telescopes of the Palomar and Anglo-Australian (AAO) observatories. All $6.4^\circ \times 6.4^\circ$ plates were digitized at the STScI (Space Telescope Science Institute) utilizing modified PDS type scanning machines (15 μm/pixel, i.e. 1 arcsec/pixel). This GSC-II database, from which the public GSC2.2 catalogue was exported, contains multi-epoch positions, multi-band magnitudes, and classification for ∼1 billion objects to $B_J \simeq 21.5$ mag derived from the analysis of ∼8000 plates (McLean et al. 2000). Table 1 shows the main characteristics of the material utilized for the construction of the GSC-II. For each survey we report the observation epochs, the photographic emulsion and filter that define the passband, and the magnitude limit. For our survey we used 32 regions of the Northern hemisphere ($\delta \gtrsim 0^\circ$), selected at high galactic latitudes in order to avoid crowding, and concentrated towards the North Galactic Pole (NGP). Figure 1 shows the distribution of the 32 regions. The total area covered is about 1150 square degrees. For each region we used three second epoch plates (POSS-II blue, red and infrared) and two first epoch plates (POSS-I blue and red), and occasionally the Quick V and ER plates. To detect high proper motion objects, we chose regions having overlapping POSS-II plates with epoch difference of $\Delta t \sim 1-10$ yr. Most of these plates were reprocessed with the same pipeline used for the construction of the GSC-II, in order to take advantage of the latest photometric calibration available to the project. In other cases, the data were extracted directly from the GSC-II database (e.g. the POSS-I plates used to improve the precision of the proper motions). Then, the object matching and proper motion evaluation was performed using the procedure described in Spagna et al. (1996).

Table 1. Main characteristics of the plate material utilized for the construction of the GSC-II.

Survey	Epoch	Emulsion +filter	Band	Depth
Pal-QV	1983–85	IIaD+W12	V_{12}	19.5
SERC-J	1975–87	IIIaJ+GG395	B_J	23.0
SERC-EJ	1979–88	IIIaJ+GG395	B_J	23.0
POSS-I E	1950–58	103aE+red	E	20.0
POSS-I O	1950–58	103aO	O	21.0
POSS-II J	1987–00	IIIaJ+GG385	B_J	22.5
POSS-II F	1987–99	IIIaF+RG610	R_F	20.8
POSS-II N	1989–02	IV-N +RG9	I_N	19.5
AAO-SES	1990–00	IIIaF+OG590	R_F	22.0
SERC-ER	1990–98	IIIaF+OG590	R_F	22.0
SERC-I	1990–02	IV-N +RG715	I_N	19.5
M W Atlas	1978–85	IV-N +RG715	I_N	19
SERC QV	1987–88	IIaD +GG495	V_{495}	14
AAO SR	1996–99	IIIaF+OG590	R_F	20

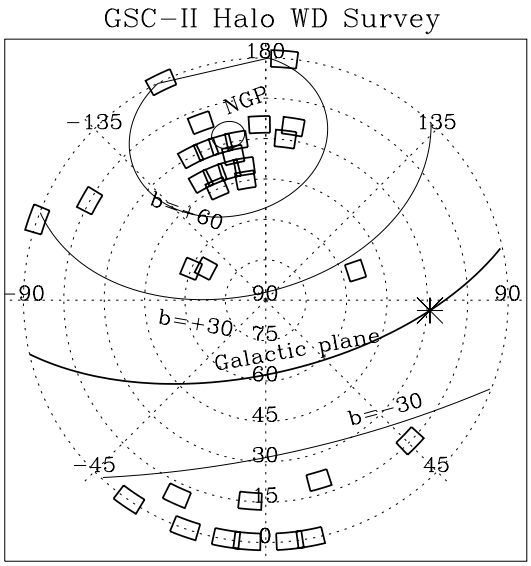

Fig. 1. Distribution of the GSC-II fields (boxes) in equatorial coordinates. Lines show the location of the NGP, the galactic plane and the strips at $b = \pm 30^\circ$ and $b = +60^\circ$.

2.1. Astrometric and photometric calibrations

Object positions were computed by means of astrometric calibrations based on the reference stars extracted from the Tycho-2 catalogue (Hog et al. 2000). A quadratic polynomial was adopted to model the transformation from the plate coordinates x, y, previously corrected for refraction, to the standard coordinates from which object positions α, δ were derived. Also, the typical distorsions which affect Schmidt plates were corrected by means of astrometric masks which model the 2D pattern of the position residuals with respect to the reference catalog as derived from the average of about 100 plates. The final accuracy of the absolute astrometry is better than 0.″2–0.″3, while relative astrometry has an accuracy of 0.″1. The photometric calibrators used for GSC-II are the GSPC-II, GSPC-I and Tycho catalogs, which sample, respectively, the faint, bright, and very bright range of the GSC-II photographic magnitudes (Bucciarelli et al. 2001). A photometric accuracy of 0.1−0.2 mag is generally attained. Larger errors may be present for faint objects close to the magnitude limit of the plate.

2.2. Proper motions

Initially, relative proper motions were derived from POSS-II plates only (epoch difference between 1−10 years) by applying the procedure described in Spagna et al. (1996). In practice, faint field stars ($R_{\rm F} \simeq 17-18$) have been selected and used as reference stars to fit a third order polynomial and transform the instrumental coordinates x, y from the secondary plates to the reference plate, usually the one at intermediate epoch. Then, relative proper motions μ_x, μ_y were computed from the multi-epoch positions by means of a linear fit. Given a position accuracy of $\sigma_{x,y} \simeq 0.1''$, the POSS-II plates provide proper motions with a typical accuracy, $\sigma_{\mu_{x,y}} \simeq \sigma_x/\Delta T$, of a few hundredths of arcsec per years which is sufficient for the identification of high proper motion objects and the selection of our targets. For the candidates confirmed by the spectroscopic follow-up (Table 2) final and more accurate proper motions were computed by using multi-epoch positions derived from a larger set of plates including the first epoch POSS-I, the intermediate epoch Quick-V, the second epoch POSS-II and ER (for the equatorial fields) (cf. Table 1). In order to cross-match the objects on all these plates, the short baseline proper motions previously computed were used to predict their position at the different epochs. Thanks to the ∼40 years between POSS-I and POSS-II plates, the typical precision of the final proper motions is $\sigma_\mu \sim 3$ mas yr^{-1} down to $R_{\rm F} \simeq 18$. Finally, absolute proper motions were derived by forcing the extragalactic sources to have a null tangential motion.

As an external check we compared the final proper motions of the targets in Table 2 with values from USNO-B. The measurements of the two catalogues appear well correlated, a part few outliers possibly due to wrong USNO-B solutions. The rms on the total proper motion difference is about $\sigma_{\Delta\mu} \simeq 8$ mas yr^{-1}, after rejecting 7 objects with large proper motion difference ($|\Delta\mu_{\alpha,\delta}| > 100$ mas yr^{-1}) and large internal errors ($\sqrt{{\sigma_{\mu\alpha}}^2 + {\sigma_{\mu\delta}}^2} > 20$ mas yr^{-1}).

3. Selection of the candidates

Cool halo WDs are not easy to observe because they are quite faint. In fact, theoretical cooling tracks by Chabrier et al. (2000) for hydrogen atmosphere WDs predict an absolute magnitude of $M_R = 15.6$ and 16.6 for a 0.6 $M_\odot$ WD of 10 and 13 Gyr respectively (excluding the nuclear burning phases). Objects of these magnitude are in reach only within a few tens of parsecs with the GSC-II material which contains objects down to the plate limits of 22.5, 20.8, and 19.5 mag for the blue B_J, red $R_{\rm F}$, and infrared I_N plates, respectively. In total we reprocessed 160 plates using the standard software pipeline which provided astrometry and photometry. As mentioned in Sect. 2.2 we identified high proper motion objects using the three second epoch plates with epoch difference between 1 yr and 10 yr.

After selecting a reference plate, usually that of intermediate epoch, objects on different plates were matched with a variable search radius, which grew as a function of the epoch difference, so as to include objects moving up to 2.5″ yr^{-1}. Their relative proper motions were then derived. To minimize false candidates, we selected only objects which were matched on all three POSS-II plates.

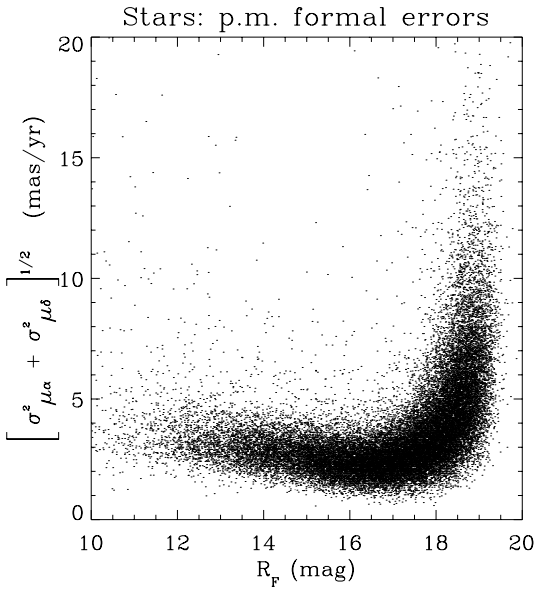

Fig. 2. Final proper motion errors as a function of magnitude for one of the field towards the NGP included in this study.

White dwarf candidates were selected by means of various criteria. We searched for faint ($R_{\rm F} \gtrsim 16$) and fast moving stars ($0.28 < \mu < 2.5''$ yr^{-1})[1]. Assuming that our survey is efficient down to $R_{\rm F} \simeq 19.0-19.5$ (i.e. 1.0−1.5 mag brighter than the plate limit), we can detect ancient and faint WDs with $M_R \simeq 16.5$ up to 30−40 pc. At this distance range, the imposed proper motion limits select objects moving with tangential velocities in the interval $40 \lesssim V_{\rm tan} \lesssim 470$ km s^{-1}, which includes almost all halo WDs and a large fraction of the thick disk WDs.

The previous criteria were implemented by means of an automatic procedure which screens the $\sim 10^5$ objects typically available in each field and provides a list of a few hundred high proper motion candidates. However, not all the selected targets had a real proper motion due to mismatches, binaries, etc. Also, the proper motion of the faintest objects were considered suspicious, due to the sudden increase of the proper motion error close to the magnitude limit of the plate. For these reasons the proper motion of each preliminary candidates was confirmed by visual inspection of the POSS-I and POSS-II plates. Finally, a cross-correlation with other catalogues (2MASS, LHS, NLTT, SDSS) was also performed.

A very useful parameter to further *refine* target selection and separate candidates WDs from (sub)dwarfs is the reduced proper motion (RPM), H, defined as (Luyten 1922)

$$H = m + 5\log\mu + 5 = M + 5\log V_{\rm tan} - 3.38 \quad (1)$$

[1] After the evaluation of the final absolute proper motion of the confirmed WDs (see Table 2), a few objects resulted moving with $\mu < 0.28''$ yr^{-1}. This is due to the relatively large error of the short baseline proper motions (POSS-II plates only), which were used for the selection of the candidates; in some cases these are objects close to the plate edge. Also, improved photometry resulted in few objects slightly brighter than $R_{\rm F} = 16$.

where m is the apparent magnitude of the star, μ ($''$/yr) is the proper motion, M is the absolute magnitude, and $V_{\rm tan}$ (km s^{-1}) is the tangential velocity. High values of H means faint and/or fast moving stars.

The reduced proper motion, used in combination with colors, is very powerful in separating the different population of the Galaxy. This is evident in Fig. 3 (left panel), which shows the RPM diagram for one of the GSC-II regions located towards the NGP. Here, the dots represent *all* the stars found in the field (i.e. without any proper motion selection), and we notice that they are clustered in two main populations. The group of objects on the top right part of the diagram is composed of late type disk dwarfs, while the population on the left with $B_J - R_{\rm F} \approx 1.0$ is mostly subdwarfs.

White dwarfs are located on the bottom left part of the RPM diagram[2]. This classification is confirmed by the position of the stellar isochrones and WD cooling tracks shown in Fig. 3. The solid and dotted lines on the top right part of the diagram show the loci of the disk dwarfs and of the halo subdwarfs based on the 10 Gyr isochrones down to 0.08 $M_\odot$ of Baraffe et al. (1997, 1998) with $[M/H] = 0$ and -1.5, respectively. Theoretical isochrones were converted to photographic magnitudes B_J and $R_{\rm F}$ using the color transformations adopted for the photometric calibration of the GSC-II.

The dot-dashed, dot-dot-dashed, and dashed lines are based on the cooling tracks for 0.6 $M_\odot$ WDs with hydrogen atmosphere from Chabrier et al. (2000). They were obtained by adopting tangential velocities of 38, 80, and 270 km s^{-1}, for the thin disk, thick disk and halo, respectively[3].

The shape of the cooling tracks reflects the recent improvement of the theory of atmosphere of cool WDs. In case of a pure hydrogen atmosphere, the cooling sequence turns back toward the blue. This effect is due to the collision-induced-absorption (CIA) in the infrared produced by molecular hydrogen (H_2) which gives a redistribution of the flux toward shorter wavelength, and is strongly present at temperatures $T_{\rm eff} < 4000$ K (see, e.g., Chabrier et al. 2000).

The right panel in Fig. 3 shows the reduced proper motion diagram for all of the objects selected, in the 1150 square degrees surveyed, after the application of the selection procedures just described. This RPM diagram was utilized to refine the sample of WDs candidates for spectroscopic follow-up. To separate WDs from contaminating (sub)dwarfs, we used as boundary line the cooling sequence for pure hydrogen atmosphere WDs (0.6 $M_\odot$) with the mean tangential velocity of the thin disk fixed at the value in the direction of the NGP; this in practice, corresponds to a kinematic selection of WDs faster than 38 km s^{-1}. Besides a significant fraction of thin disk WDs, such threshold includes almost all of the WDs with halo kinematics and most of the thick disk WDs[4].

We observed all the candidates lying below the boundary line; a few objects above the threshold and some candidates with $B_J - R_{\rm F}$ redder than the cooling track turnoff ($B_J - R_{\rm F} \simeq 1.7$) were also observed in order to check the efficiency of the selection criteria and to take into account the photometric error.

In the figure, dots are used for the stars in the initial candidate sample which were later excluded from the spectroscopic follow-up list; confirmed WDs are plotted as triangles, while (sub)dwarfs are represented as asterisks. We note that all the confirmed WDs (except a couple of cases with slightly redder color) fall under the boundary line, while the contaminating (sub)dwarfs are distributed near the threshold. These results demonstrate the good quality of the data, the selection criteria and the accuracy of our final sample.

4. Observations and data reduction

Low dispersion spectra were measured to confirm the nature of the selected candidates and remove possible contaminants, like (sub)dwarfs.

The bulk of the spectroscopic follow-up was carried out at the 3.5 m Telescopio Nazionale Galileo (TNG, La Palma), with additional contribution of the service programmes of the 4.2 m William Herschel Telescope and the 2.4 m Isaac Newton Telescope (WHT and INT, La Palma).

We used the low resolution spectrograph DOLORES (Device Optimized for LOw RESolution) installed at the Naysmith B focus of the TNG. Half of our spectra were measured on the nights of April 16th−18th 2002, conditions were mostly good, the first half of the first night suffered seeing of around 2 arcsec, but this settled down over the rest of the run to be 1−1.5 arcsec. The remaining objects were measured in a second run on October 2002, in service time on February 2003 and in service time from August 2003 to January 2004. Most of our spectra were observed with the low resolution, blue-optimized Grism 1 (or LR-B) with a long slit. The transmission of the LR-B grism peaks at around 400−500 nm with a central weavelength of 585.0 nm and useful coverage from 300 nm to 880 nm and a dispersion of 2.8 Å per pixel. The camera is equipped with a 2048 × 2048 Loral thinned and back-illuminated CCD with 15 micron pixels. The field of view is 9.38 × 9.38 arcmin with a 0.275 arcsec/pix scale, hence a 1 arcsec slit projects to 3.6 pixels, or a resolution of ∼11 Å. Most of our targets were observed with a 1.0 arcsec slit; on April 15th when seeing was poor we employed the 1.5 arcsec slit and the 2.0 arcsec slit. Each target was pre-imaged to define its exact position (helpful with such high

[2] Notice that most of the objects with $H \approx 25$ are not real, and were rejected by the application of the selection criteria and visual inspection.

[3] Those numbers represent mean values computed numerically assuming the velocity ellipsoids $(\sigma_U, \sigma_V, \sigma_W; v_a) = (34, 21, 18; -6)$ for the thin disk (Binney & Merrifield 1998, Table 10.4), $(63, 39, 39; -45)$ for the thick disk (Soubiran et al. 2003), and $(160, 89, 94; -217)$ for the halo (Casertano et al. 1990). Also, a solar motion $(U, V, W) = (10.0, 5.25, 7.17)$ km s^{-1} is adopted from Dehnen & Binney (1998).

[4] The exact fraction of selected objects is a function of the line of sight because it depends on the projection of the velocity ellipsoid. Assuming the velocity ellipsoid from Casertano et al. (1990) and Soubiran et al. (2003) respectively for the halo and thick disk, we estimated that for our fields at intermediate galactic latitudes less than 2% of the halo WDs and 20% of the thick disk WDs are moving with $V_{\rm tan} < 38$ km s^{-1}. Such fraction decreases to a minimum of 0.25% and 13% of halo and thick disk WDs in the cases of the high latitude fields towards the NGP.

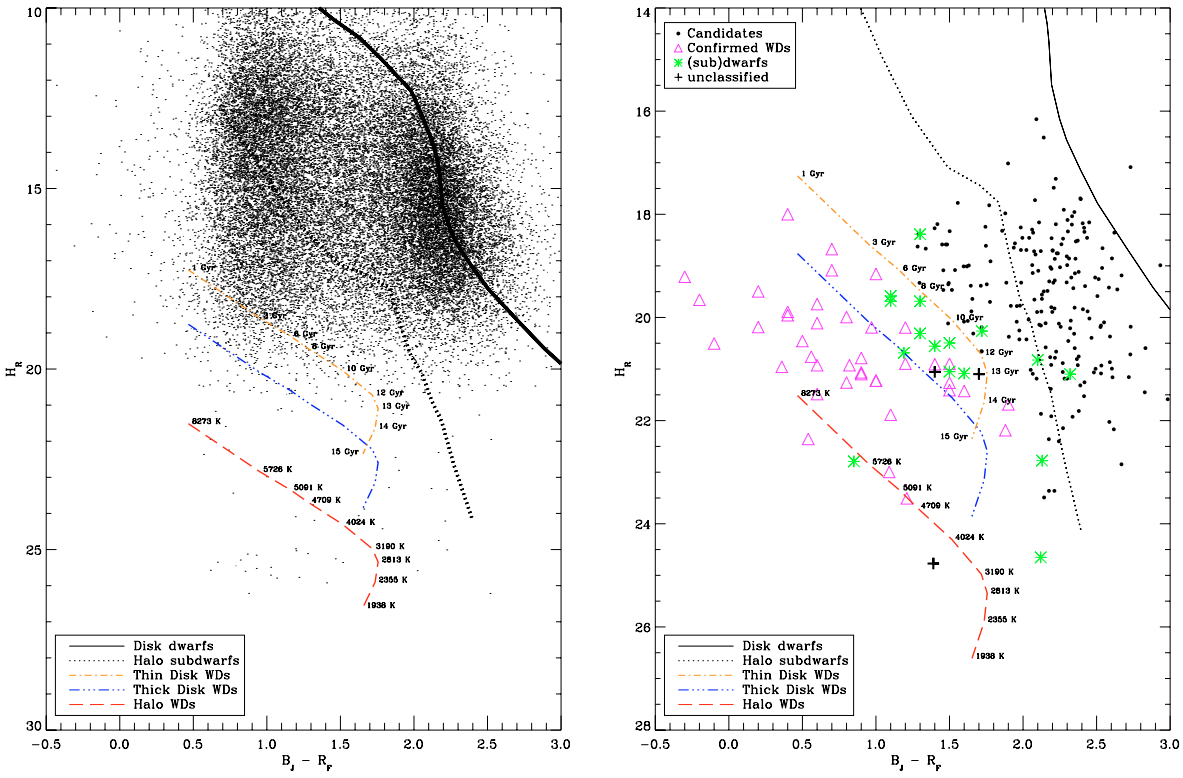

Fig. 3. *Left panel*: RPM diagram for a GSC-II region located towards the NGP. Stellar isochrones and WD cooling tracks are plotted with different lines (see text). *Right panel*: RPM diagram for all the candidates selected in the 1150 square degrees surveyed for this study. Dots show the unobserved targets, while triangles and asterisks are the spectroscopically confirmed WDs and contaminating (sub)dwarfs, respectively. Crosses indicate stars unclassified due to the low signal to noise of their spectra.

proper motion stars). Typically, an exposure time of 3600 s and 300 s was sufficient to provides a suitable signal-to-noise ratio, $S/N \geq 10$, for the faintest ($R_F \simeq 19.5$) and the brightest ($R_F \simeq 16$) target respectively. Spectrophotometric standards were observed a few times per night to enable an approximate flux calibration, but most importantly to help get the shape of the spectrum correct. The standards were drawn from the list at `http://www.ing.iac.es/Astronomy/observing/manuals/html_manuals/tech_notes/tn065-100/workflux.html`

We measured the stars GD 140, BD+17 4708, Feige 67 and HZ 44. We obtained Helium arc lamp exposures to facilitate wavelength calibration. Halogen lamp flat fields were measured to enable us to measure the pixel-to-pixel sensitivity variations.

Spectra for 4 objects in Tables 2−4 were measured using the intermediate dispersion spectrographic and imaging system (ISIS) on the 4.2 m WHT. Observations were made during service nights on the 27th and 29th January 2001, 6th December 2003, and 3rd and 4th February 2004. ISIS is a two-arm spectrograph, employing the 5700 Å dichroic to split the blue and red light into two cameras. In the blue arm we used the R300B grating with the EEV12 CCD (4096 pixels in the wavelength direction) at a central wavelength of about 4400 Å. This setup achieves a dispersion 0.86 Å/pix and useful wavelength coverage of about 3000 Å. The slit width was matched to the seeing, typically 1 arcsec projecting to 4 detector pixels. In the red arm we used the R316R grating with the Marconi2 CCD (4610 pixels in the dispersion direction) at a central wavelength of about 6250 Å. The dispersion is 0.84 Å/pix covering 3858 Å, but around 1000 of these pixels suffer significant (50−80%) vignetting from the camera optics. Combining the red and blue arm spectra gave us spectra with useful coverage over the wavelength range 3400−8000 Å.

Spectra for 2 of the objects listed in the Tables 2−4 were measured in service time on the 2.5 m INT. We employed the (currently decommissioned) Intermediate Dispersion Spectrograph (IDS) mounted at the Cassegrain focus. Observations were made during the nights of 8th April 2003 and 19th April 2003. The instrumental setup was the same for both nights, using the 235 mm camera with the R150V grating and the EEV10 CCD. This grating and camera combination gives a dispersion of 271.3 Å mm^{-1}, which is equivalent to 3.66 Å/pixel for the EEV10 detector, and useful wavelength coverage was from approximately 3300−8700 Å. The camera and detector achieve a spatial scale of 0.4 arcsec per pixel. On the first night, the slit was opened up to 2.5 arcsec (6 pixels). On the second night we observed with a 1.0 arcsec slit (2.5 pixels). A total of 4 targets were measured on the first night, with exposure times of between 1200 and 2700 s each, as well as one standard star, SP1550+330. On the second night we observed 2 targets, each with 2 × 1800 s exposures, as well as the flux standard SP1446+259. Calibration arc lamps and flat fields were measured on both nights.

Data reduction for all spectra was performed within the IRAF and MIDAS data reduction package. The same

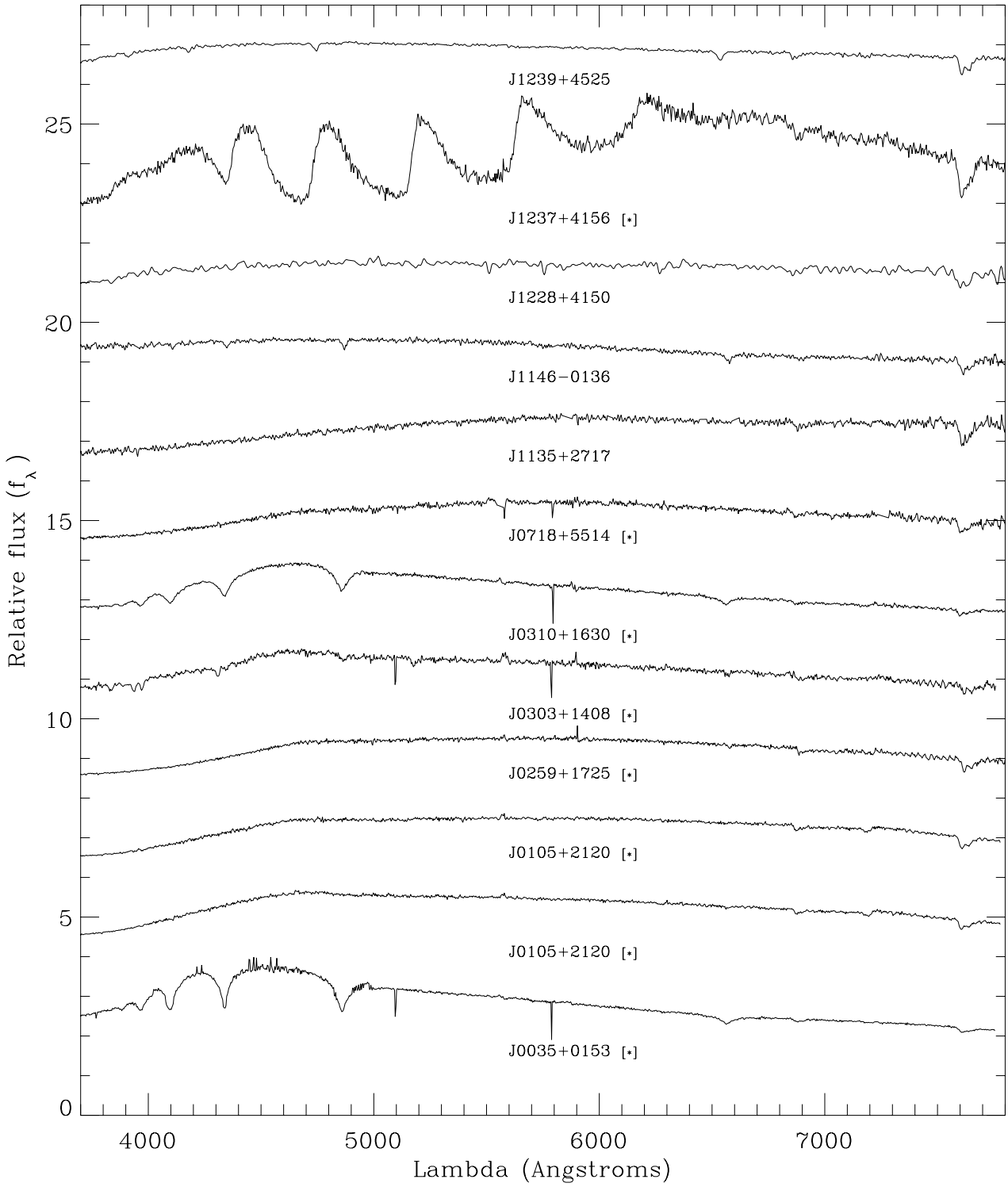

Fig. 4. Optical spectra. All the spectra are normalized at 5500 Å, shifted vertically from each other by arbitrary units, and ordered by increasing right ascension. Asterisks indicate spectra not fully calibrated, shown for classification only.

procedure was followed for all objects wherever possible, regardless of the instrument and telescope used to acquire the data. All images were debiased using a mean zero second frame. Images were then flatfielded using lamp observations to remove the pixel-to-pixel sensitivity variations. 1-D spectra were extracted and background subtracted, then wavelength calibrated using arc lamp spectra.

Most of the spectra were flux calibrated using the standard star observations, although no correction was made for extinction. 16 spectra have not been flux calibrated at this time and are presented in Figs. 4−6 in their uncalibrated form. Thus the turn-over to the blue of these objects reflects the sensitivity of the instrument, rather than the intrinsic spectral shape of the object. This does not prevent us from identifying that these stars

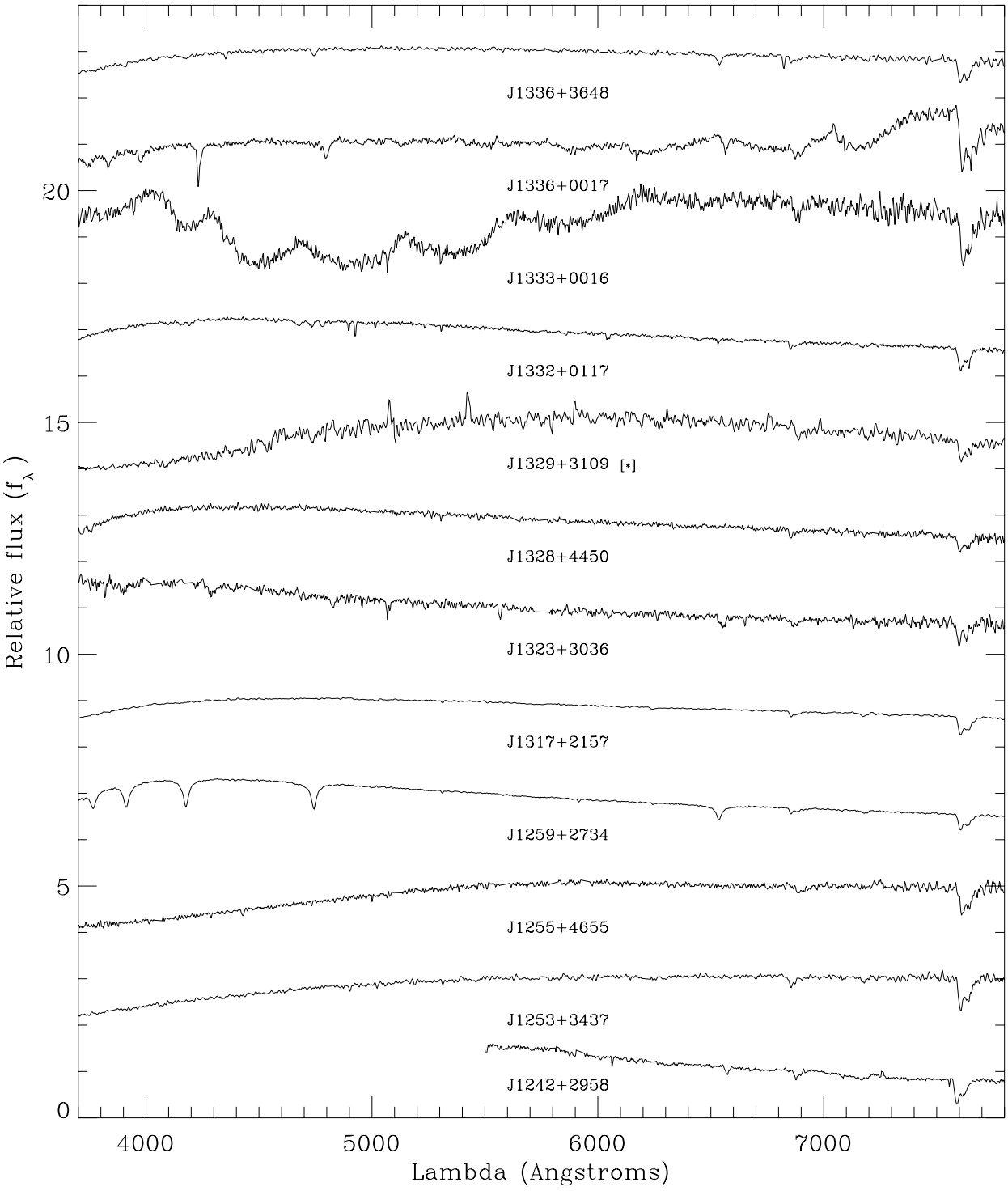

Fig. 5. Optical spectra. All the spectra are normalized at 5500 Å, shifted vertically from each other by arbitrary units, and ordered by increasing right ascension. Asterisks indicate spectra not fully calibrated, shown for classification only.

are WDs, but does caution against detailed spectral analysis at this time, which will be completed and presented in a future paper (Carollo et al., in preparation).

5. The GSC2 sample of WDs

We secured spectra for 59 candidates: 40 were confirmed WDs, 16 were a mixture of late type dwarfs and subdwarfs, while the spectra of the last 3 stars failed to reduce due to poor data quality. A couple of candidates below the boundary line (see Sect. 3) were not observed for technical reasons. One of them (LHS 1093) is a known WD (Bergeron et al. 1997). Thus, our sample counts 41 WDs in total, 17 of which show no presence of the H_α line, and two are exotic examples of DQ and DZ.

Table 2 gives the astrometry of the WD sample; Col. 1 reports the GSC-II identification, while the remaining columns

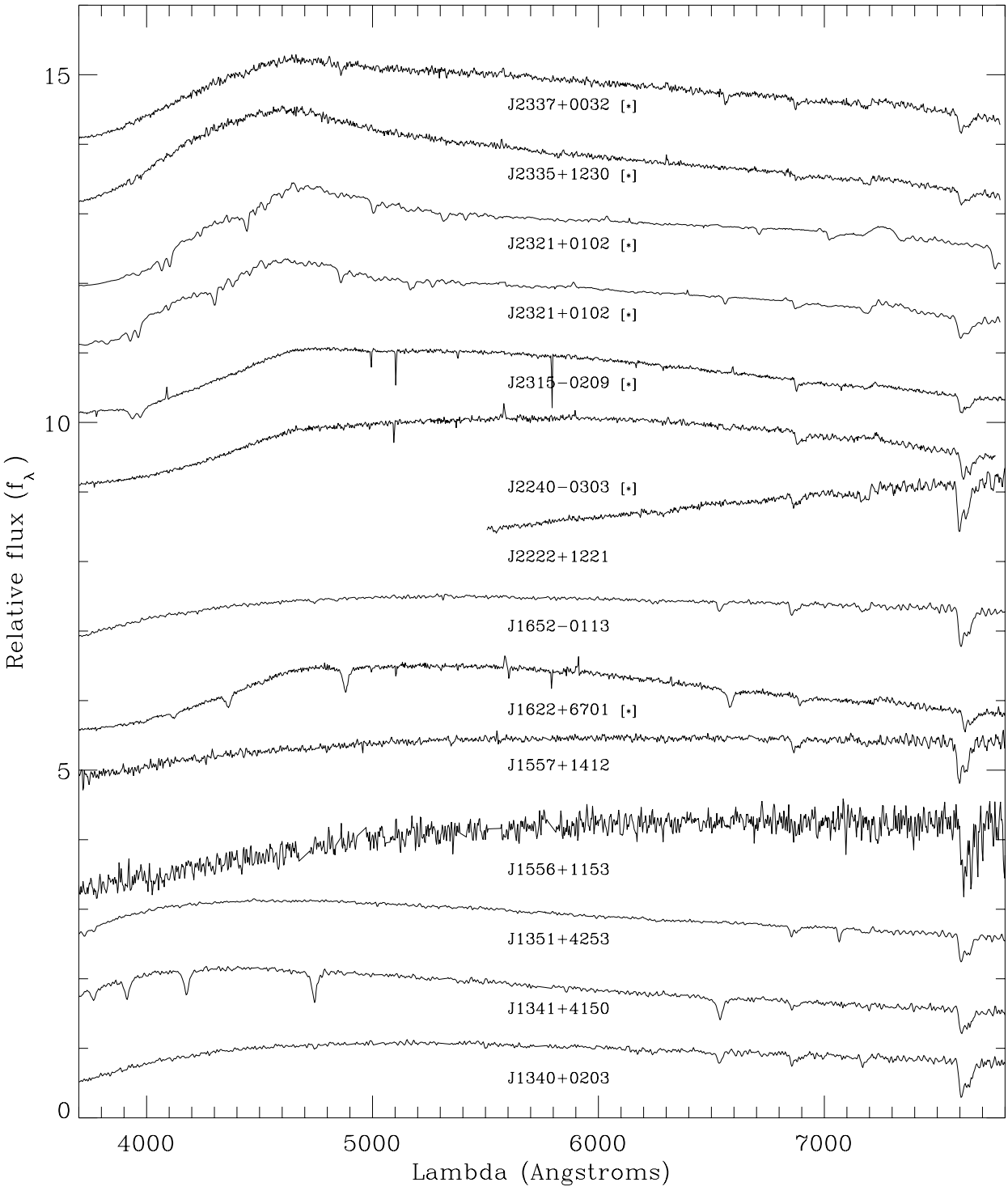

Fig. 6. Optical spectra. All the spectra are normalized at 5500 Å, shifted vertically from each other by arbitrary units, and ordered by increasing right ascension. Asterisks indicate spectra not fully calibrated, shown for classification only.

list: positions with accuracy in the range 0.2″−0.3″, absolute proper motions with a typical total error between 2 and 6 mas yr^{-1}, and the epoch of the corresponding position.

Table 3 provides B_J and R_F photometry, spectroscopic classification, and source telescope. Magnitudes are between $15.1 < R_F < 19.7$ and colors in the range $-0.10 < B_J - R_F < 1.91$. The last column of Table 3 lists the cross-identification with other WD catalogues. Only 5 objects are in common with the SDSS sample of cool WDs (Kilic et al. 2005), while 12 WDs were found in the Villanova catalogue (McCook & Sion 1999) available at CDS (`http://cdsweb.u-strasbg.fr/`). Therefore, our sample counts 24 newly discovered WDs.

Finally, Table 4 reports the cross-match with Luyten's catalogues, the Data Release 4 (DR4) of the SDSS (Adelman-McCarthy et al. 2005), and the 2MASS catalogue

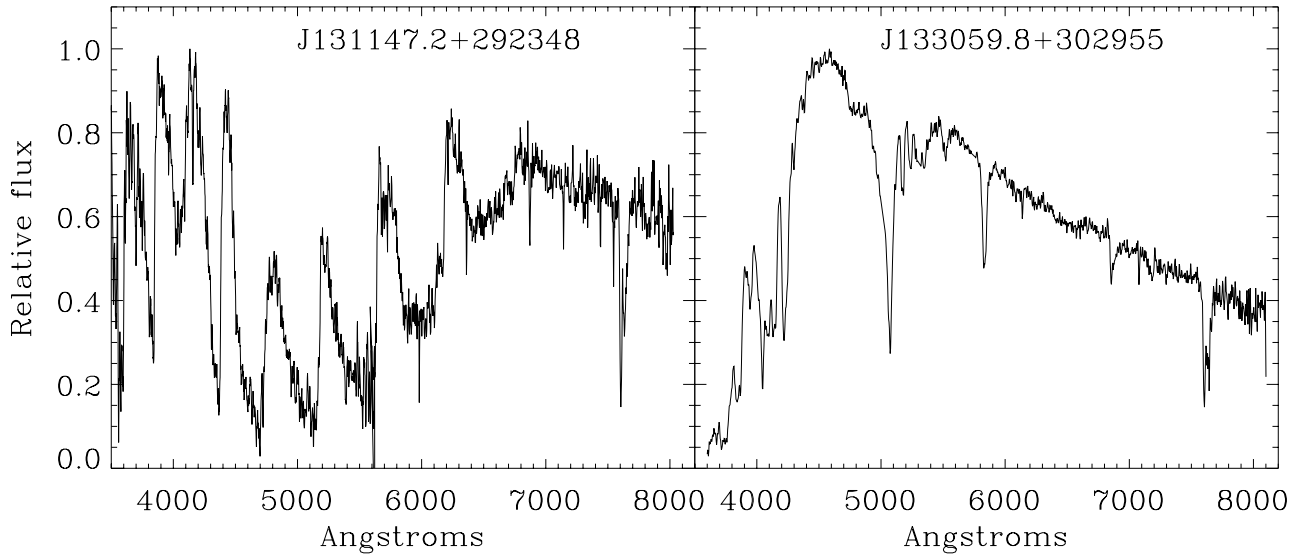

Fig. 7. Optical spectra of the peculiar WDs. *Left panel* shows GSC2U J 131147.2+292348 which is the coolest DQ with extremely strong C_2 bands. *Right panel* shows WD 1328+307 (G 165-7) which is a heavily blanketed DZ.

(Cutri et al. 2003); Col. 2 gives the NLTT/LHS identification. In the remaining columns we provide *ugriz* photometry for 19 WDs found in SDSS-DR4, and JHK_s magnitudes for 19 objects found in 2MASS.

Figures 4−6 show the optical spectra of the WDs in the GSC-II sample[5], except for the two peculiar WDs, plotted in Fig. 7. Of the 41 WDs, 17 are featureless (DC) and 19 are DA. Two stars in the sample (LHS 5222 and LP 618-6) show carbon features and one of them (LP 618-6) is magnetic (Schmidt et al. 2003).

Two stars (GSC2U J030339.2+140805 and LP 618-14) show the features of a composite spectrum which indicates the presence of a red companion. A third star (LP 618-1) is an unresolved degenerate double formed by a magnetic DA and a massive DC (Bergeron et al. 1993).

Also, we found 2 common proper motion systems composed of WDs only (LHS 5023 + LHS 5024 and LP 642-52 + LP 642-53). White dwarf GSC2U J071859+551406 is the faint component of another common proper motion pair with G 193-40 as the bright companion.

The left panel in Fig. 7 shows the coolest (5120 K) carbon rich WD known to date: GSC2U J131147.2+292348 described in Carollo et al. (2002, 2003). Another similar DQ was recently discovered in the SDSS (Kleinman et al. 2004); its modelling by Dufour et al. (2005) yields a temperature of 5140 K, which increases to two the DQs with temperature below the expected cutoff of 6000 K.

The right panel shows the spectrum of GSC2U J133059.8+302955 (G 165-7) which is a peculiar DZ with an estimated temperature of 7500 K (Wehrse & Liebert 1980).

[5] The spectra of the two WDs GSC2U J124212.6+295801 and GSC2U J222233.1+122140 have a reduced wavelength coverage as they were observed at the TNG with a different Grism (LR-R).

6. Conclusions

We have presented a new high proper motion survey to search for ancient cool WDs. The survey is based on the GSC-II material and covers an area of about 1150 square degrees. Using appropriate selection criteria, the RPM diagram, and spectroscopic follow-up, we identified 41 WDs, 17 of which show no H_α line, and two of peculiar nature.

This new and independent WD sample will be used to infer new constraints on the halo WD space density (Carollo et al., in preparation) by means of a new method to separate thick disk from halo WDs based on the kinematic properties of the candidates (Spagna et al. 2004). Furthermore, this sample will be useful to increase the statistics of such rare objects and provide information on the age of thick disk and halo through the analysis of the luminosity function.

Acknowledgements. The GSC-II is a joint project of the Space Telescope Science Institute and the INAF-Osservatorio Astronomico di Torino. Space Telescope Science Institute is operated by AURA for NASA under contract NAS5-26555. Partial financial support to this research cames from the Italian CNAA and the Italian Ministry of Research (MIUR) through the COFIN-2001 program. This work is based on observations made with the Italian Telescopio Nazionale Galileo (TNG) operated on the island of La Palma by the Centro Galileo Galilei of the INAF (Istituto Nazionale di Astrofisica) at the Spanish Observatorio del Roque de los Muchachos of the Instituto de Astrofisica de Canarias, and also based on observations made with the William Herschel Telescope and the Isaac Newton Telescope operated on the island of La Palma by the Isaac Newton Group in the Spanish Observatorio del Roque de los Muchachos of the Instituto de Astrofisica de Canarias.

Special thanks to C. Loomis, A. Volpicelli and A. Zacchei for their valuable technical support to this project and to D. Koester for the many useful discussions. Finally, B.B. and M.G.L. acknowledge the support of the STScI through the Institute's Visitor Program for 2005.

References

Adelman-McCarthy, K. J., et al. 2005 [arXiv:astro-ph/0507711]
Afonso, C., Albert, J. N., Alard, C., et al. 2003, A&A, 404, 145
Alcock, C., Allsman, R. A., Alves, D. R., et al. 2000, ApJ, 542, 281
Baraffe, I., Chabrier, G., Allard, F., & Hauschildt, P. H. 1997, A&A, 327, 1054
Baraffe, I., Chabrier, G., Allard, F., & Hauschildt, P. H. 1998, A&A, 337, 403
Bergeron, P., Ruiz, M. T., & Leggett, S. K. 1993, ApJ, 407, 733
Bergeron, P., Ruiz, M. T., & Leggett, S. K. 1997, ApJS, 108, 339
Binney, J., & Merrifield, M. 1998, Galactic Astronomy (Princeton Univ. Press)
Bucciarelli, B., García Yus, J., Casalegno, R., et al. 2001, A&A, 368, 335
Carollo, D., Hodgkin, S. T., Spagna, A., et al. 2002, A&A, 393, L45
Carollo, D., Koester, D., Spagna, A., Lattanzi, M. G., & Hodgkin, S. T. 2003, A&A, 400, L13
Casertano, S., Ratnatunga, K. U., Bahcall, J. N., et al. 1990, ApJ, 357, 435
Chabrier, G., Brassard, P., Fontaine, G., & Saumon, D. 2000, ApJ, 543, 216
Cutri, R. M., et al. 2003, 2MASS All-Sky Catalog of Point Sources (Pasadena: Caltech)
Dehnen, W., & Binney, J. 1998, MNRAS, 298, 387
Dufour, P., Bergeron, P., & Fontaine, G. 2005, ApJ, 627, 404
Hansen, Brad, M. S., & Liebert, J. 2003, ARA&A, 41, 465
Hög, E., Fabricius, C., Makarov, V. V., et al. 2000, A&A, 355, 27
Kilic, M., Munn, J. A., Harris, H. C., et al. 2005, AJ, in press [arXiv:astro-ph/0503601]
Kleinman, S. J., Harris, H. C., Eisenstein, D. J., et al. 2004, ApJ, 607, 426
Luyten, W. J. 1922, PASP, 34, 54
Luyten, W. J. 1979, NLTT, Minneapolis, Univ. of Minnesota
McCook, G. P., & Sion, E. M. 1999, ApJS, 121, 1
McLean, B. J., Greene, G. R., Lattanzi, M. G., & Pirenne, B. 2000, in ADASS IX, ASP Conf. Ser., 216, 145
Monet, D. G., Dahn, C. C., Vrba, F. J., et al. 1992, AJ, 103, 638
Nguyen, Hien, T., Kallivayalil, N., Werner, M. W., et al. 2004, ApJS, 154, 266
Pacynski, B. 1986, ApJ, 304, 1
Reid, I. N. 2005, ARA&A, 43, 247
Schmidt, G. D., Harris, H. C., Liebert, J., et al. 2003, ApJ, 595, 1101
Soubiran, C., Bienaymé, O., Siebert, A., et al. 2003, A&A, 398, 141
Spagna, A., Lattanzi, M. G., Lasker, B. M., et al. 1996, A&A, 311, 758
Spagna, A., Carollo, D., Lattanzi, M. G., & Bucciarelli, B. 2004, A&A, 428, 451
Tisserand, P., & Milsztajn, A. 2005, Proc. of the 5th Rencontres du Vietnam, Hanoi, Aug. 5−11, 2004 [arXiv:astro-ph/0501584]
Wehrse, R., & Liebert, J. 1980, A&A, 86, 139

Online Material

Table 2. The sample of cool WDs from the GSC-II survey: astrometric parameters.

ID	RA (J2000)	Dec (J2000)	$\mu_\alpha \cos\delta$ mas yr^{-1}	μ_δ mas yr^{-1}	Epoch
GSC2U J003209.6−025402	00 32 09.57	–02 54 02.6	630.4 ± 4.4[a]	−149.5 ± 4.3[a]	1993.85
GSC2U J003536.0+015314	00 35 35.97	+01 53 14.0	−139.0 ± 1.5	−361.2 ± 1.3	1991.76
GSC2U J010456.6+212002	01 04 56.62	+21 20 02.0	−208.4 ± 2.9	−434.1 ± 2.8	1991.63
GSC2U J010458.1+212021	01 04 58.10	+21 20 21.0	−205.7 ± 2.8	−437.4 ± 2.5	1991.63
GSC2U J025936.9+172533	02 59 35.86	+17 25 33.0	−271.4 ± 8.5[a]	−93.5 ± 7.8[a]	1991.79
GSC2U J030339.2+140805	03 03 39.15	+14 08 05.0	50.8 ± 1.9[b]	−477.4 ± 35.5[b]	1991.79
GSC2U J031000.4+163022	03 10 00.43	+16 30 22.0	208.5 ± 4.1[a]	−193.3 ± 4.4[a]	1991.79
GSC2U J071858.8+551406	07 18 58.80	+55 14 06.0	161.7 ± 3.9	−191.6 ± 7.8	1989.93
GSC2U J113524.7+271741	11 35 24.72	+27 17 41.4	−349.4 ± 4.0	−62.5 ± 3.8	1995.31
GSC2U J114625.7−013635	11 46 25.68	–01 36 34.8	351.8 ± 0.6	−433.7 ± 1.4	1995.00
GSC2U J122810.3+415003	12 28 10.32	+41 50 03.5	−262.9 ± 4.5	64.8 ± 5.2	1988.22
GSC2U J123752.6+415622	12 37 52.56	+41 56 22.4	−337.2 ± 2.8	340.6 ± 0.7	1988.22
GSC2U J123915.4+452520	12 39 15.36	+45 25 20.4	−637.1 ± 1.7	−530.5 ± 3.1	1988.22
GSC2U J124212.6+295801	12 42 12.57	+29 58 00.6	−515.1 ± 4.2	−350.9 ± 19.8	1990,08
GSC2U J125313.0+343712	12 53 12.96	+34 37 11.7	−303.9 ± 7.6	161.2 ± 2.1	1990.21
GSC2U J125509.6+465520	12 55 09.60	+46 55 19.9	−1087.9 ± 2.7	−84.2 ± 3.8	1988.22
GSC2U J125946.8+273404	12 59 46.80	+27 34 03.6	−311.5 ± 10.4	81.3 ± 8.6	1993.29
GSC2U J131147.2+292348	13 11 47.28	+29 23 47.4	−384.9 ± 2.5[c]	320.3 ± 4.2[c]	1995.23
GSC2U J131749.0+215715	13 17 48.98	+21 57 14.7	−26.9 ± 1.9	−274.8 ± 1.6	1996.30
GSC2U J132325.2+303615	13 23 25.20	+30 36 15.3	−101.6 ± 2.4	−405.2 ± 5.3	1995.31
GSC2U J132857.4+445034	13 28 57.36	+44 50 34.5	106.4 ± 2.7	−223.6 ± 3.1	1994.42
GSC2U J132909.6+310947	13 29 09.60	+31 09 47.2	−244.8 ± 3.7	89.1 ± 0.7	1995.31
GSC2U J133059.8+302955	13 30 59.76	+30 29 55.1	−471.9 ± 2.1	−107.5 ± 1.8	1995.31
GSC2U J133250.9+011707	13 32 50.88	+01 17 07.2	13.4 ± 1.6	−274.6 ± 2.1	1996.23
GSC2U J133360.0+001654	13 33 60.00	+00 16 54.3	−328.9 ± 2.0	206.1 ± 2.0	1996.22
GSC2U J133616.1+001733	13 36 16.08	+00 17 33.0	−280.0 ± 0.9	−139.8 ± 1.3	1996.23
GSC2U J133620.4+364829	13 36 20.40	+36 48 29.2	−248.4 ± 5.3	222.5 ± 4.1	1996.22
GSC2U J134043.4+020348	13 40 43.44	+02 03 48.2	−531.3 ± 2.3	31.5 ± 0.9	1996.23
GSC2U J134107.9+415004	13 41 07.92	+41 50 04.5	−217.0 ± 1.4	−188.7 ± 3.3	1996.22
GSC2U J135118.4+425317	13 51 18.35	+42 53 16.8	213.7 ± 2.8	−253.8 ± 3.8	1994.42
GSC2U J155611.5+115351	15 56 11.52	+11 53 51.4	−193.1 ± 3.7	26.0 ± 6.0	1994.42
GSC2U J155721.8+141212	15 57 21.75	+14 12 11.9	−204.7 ± 1.4	−244.2 ± 4.8	1994.44
GSC2U J162242.0+670112	16 22 42.00	+67 01 12.3	−76.2 ± 3.6	181.5 ± 2.8	1994.42
GSC2U J165237.4−011354	16 52 37.44	–01 13 54.5	131.3 ± 1.7	−359.1 ± 0.9	1990.40
GSC2U J222233.1+122140	22 22 33.12	+12 21 40.3	706.3 ± 2.3	185.5 ± 2.4	1987.72
GSC2U J224011.2−030316	22 40 11.25	–03 03 16.0	−202.1 ± 5.3	−217.7 ± 2.3	1995.59
GSC2U J231518.5−020942	23 15 18.48	–02 09 42.0	578.4 ± 2.1	169.5 ± 1.3	1990.66
GSC2U J232115.4+010214	23 21 15.36	+01 02 14.4	−104.6 ± 2.4	−244.8 ± 1.9	1990.66
GSC2U J232116.8+010227	23 21 15.84	+01 02 27.0	−98.0 ± 6.6	−242.5 ± 3.3	1990.66
GSC2U J233539.1+123048	23 35 39.12	+12 30 48.2	−111.3 ± 1.5	−134.1 ± 1.9	1995.82
GSC2U J233707.4+003240	23 37 07.44	+00 32 40.3	299.7 ± 1.9	158.5 ± 1.6	1990.74

[a] Proper motions computed from POSS-I, SERC-J, SERC-ER, and SERC-I positions (α, δ) extracted from the GSC-II database.
[b] Proper motions computed from POSS-II positions (α, δ) extracted from the GSC-II database (ΔT = 6.0 years).
[c] The value ($\mu_\delta = 0.286''$ yr^{-1}) reported in Carollo et al. (2002) was affected by a systematic error. We report here the updated value.

Table 3. The sample of cool WDs from the GSC-II survey: photometry, classification, source telescope, WD ID in other catalogues.

ID	B_J	R_F	$B_J - R_F$	Type	Source	WDs ID
GSC2U J003209.6−025402	17.78	16.51	1.27	DA	[a]	WD 0029-032
GSC2U J003536.0+015314	15.78	15.70	0.08	DA	TNG	WD 0033+016
GSC2U J010456.6+212002	18.60	17.42	1.18	DC	TNG	WD 0102+210A
GSC2U J010458.1+212021	18.90	17.52	1.38	DC	TNG	WD 0102+210B
GSC2U J025936.9+172533	19.61	19.06	0.55	DA	TNG	
GSC2U J030339.2+140805	20.63	19.54	1.09	DA+dM	TNG	
GSC2U J031000.4+163022	18.04	17.85	0.19	DA	TNG	
GSC2U J071858.8+551406	20.84	19.71	1.13	DC	WHT	
GSC2U J113524.7+271741	19.13	18.22	0.91	DC	TNG	
GSC2U J114625.7-013635	16.53	15.98	0.55	DA	TNG	SDSS J114625.77-013636.9
GSC2U J122810.3+415003	19.24	18.42	0.82	DC	TNG	
GSC2U J123752.6+415622	17.83	16.70	1.13	DQ	TNG/INT	
GSC2U J123915.4+452520	16.83	16.27	0.56	DA	TNG	WD 1236+457
GSC2U J124212.6+295801	18.34	17.75	0.58	DA	TNG	
GSC2U J125313.0+343712	19.90	18.41	1.49	DC	TNG	
GSC2U J125509.6+465520	19.49	18.28	1.21	DC	TNG	
GSC2U J125946.8+273404	15.55	15.13	0.42	DA	TNG	WD 1257+278
GSC2U J131147.2+292348	19.56	18.04	1.52	Peculiar DQ[b]	WHT	
GSC2U J131749.0+215715	17.30	16.59	0.71	DC	TNG	
GSC2U J132325.2+303615	19.89	19.35	0.54	DA	TNG	
GSC2U J132857.4+445034	18.57	18.04	0.53	DC	TNG	
GSC2U J132909.6+310947	21.23	19.32	1.91	DC	TNG/WHT	
GSC2U J133059.8+302955	16.62	15.75	0.87	Peculiar DZ[c]	TNG	WD 1328+307
GSC2U J133250.9+011707	17.34	16.65	0.69	DC+DA[d]	TNG	WD 1330+015 (A+B)
GSC2U J133360.0+001654	19.50	17.98	1.52	DQ	TNG/INT	WD1331+005
GSC2U J133616.1+001733	17.72	16.73	0.99	DA+dM	TNG	SDSS J133616.05+001732.7
GSC2U J133620.4+364829	18.21	17.40	0.81	DA	TNG	
GSC2U J134043.4+020348	18.38	17.60	0.78	DA	TNG	SDSS J134043.35+020348.3
GSC2U J134107.9+415004	17.95	17.52	0.43	DA	TNG	
GSC2U J135118.4+425317	17.14	16.52	0.62	DC	TNG	
GSC2U J155611.5+115351	20.51	18.94	1.57	DC	TNG	
GSC2U J155721.8+141212	19.43	18.06	1.37	DC	TNG	
GSC2U J162242.0+670112	18.89	18.99	–0.10	DA	TNG/WHT	
GSC2U J165237.4−011354	17.87	16.69	1.18	DA	TNG	
GSC2U J222233.1+122140	19.74	17.87	1.87	DC	TNG	SDSS J222233.90+122143.0
GSC2U J224011.2−030316	18.95	17.79	1.16	DC	TNG	
GSC2U J231518.5−020942	16.39	16.00	0.39	DZ	TNG	WD 2312-024
GSC2U J232115.4+010214	19.62	18.65	0.97	DA	TNG	WD 2318+007A
GSC2U J232116.8+010227	20.23	18.79	1.44	DC	TNG	WD 2318+007B
GSC2U J233539.1+123048	18.81	18.45	0.36	DC	TNG	
GSC2U J233707.4+003240	18.58	17.61	0.97	DA	TNG	SDSS J233707.68+003242.3

[a] Classification from Monet et al. (1992) and Bergeron et al. (1997).
[b] Peculiar DQ with extremely strong C_2 bands (Carollo et al. 2002, 2003).
[c] Heavily blanketed DZ (G 165-7) (Wehrse & Liebert 1980).
[d] Unresolved binary (DC + magnetic DA) modeled by Bergeron et al. (1997).

Table 4. The sample of cool WDs from the GSC-II survey: cross-match with Luyten's catalogues (LHS and NLTT). Photometry from SDSS and 2MASS.

	LHS/NLTT	SDSS					2MASS		
ID		*u*	*g*	*r*	*i*	*z*	*J*	*H*	*K*
GSC2U J003209.6−025402	LHS 1093	–	–	–	–	–	15.56	15.37	15.35
GSC2U J003536.0+015314	LP 585- 53	–	–	–	–	–	15.65	15.52	16.12
GSC2U J010456.6+212002	LHS 5023	–	–	–	–	–	16.52	16.50	15.55
GSC2U J010458.1+212021	LHS 5024	–	–	–	–	–	16.73	16.27	15.59
GSC2U J025936.9+172533	LP 411- 34	–	–	–	–	–	–	–	–
GSC2U J030339.2+140805	–	–	–	–	–	–	14.01	13.56	13.25
GSC2U J031000.4+163022	LP 412- 7	–	–	–	–	–	–	–	–
GSC2U J071858.8+551406	–	–	–	–	–	–	–	–	–
GSC2U J113524.7+271741	LP 318-432	–	–	–	–	–	–	–	–
GSC2U J114625.7−013635	LHS 2455	17.14	16.51	16.24	16.14	16.17	15.54	15.38	15.18
GSC2U J122810.3+415003	LP 217- 20	19.89	19.02	18.57	18.41	18.29	–	–	–
GSC2U J123752.6+415622	LHS 5222	17.85	17.75	17.11	16.85	16.93	16.55	16.50	15.48
GSC2U J123915.4+452520	LHS 2596	17.35	16.65	16.37	16.28	16.29	15.60	15.20	15.73
GSC2U J124212.6+295801	LHS 2607	–	–	–	–	–	–	–	–
GSC2U J125313.0+343712	–	–	–	–	–	–	–	–	–
GSC2U J125509.6+465520	–	21.05	19.17	18.38	18.05	17.92	–	–	–
GSC2U J125946.8+273404	LP 322- 267	–	–	–	–	–	15.13	14.98	14.99
GSC2U J131147.2+292348	–	19.70	19.45	18.50	17.94	18.00	17.48	17.13	17.08
GSC2U J131749.0+215715	LP 378- 956	–	–	–	–	–	16.03	15.79	15.96
GSC2U J132325.2+303615	–	–	–	–	–	–	–	–	–
GSC2U J132857.4+445034	–	18.79	18.41	18.33	18.34	18.40	–	–	–
GSC2U J132909.6+310947	–	–	–	–	–	–	–	–	–
GSC2U J133059.8+302955	LHS 2745	18.27	16.28	15.87	15.90	16.08	15.40	15.28	15.41
GSC2U J133250.9+011707	LP 618-1	17.72	17.13	16.95	16.91	16.92	16.40	16.30	15.80
GSC2U J133360.0+001654	LP 618- 6	19.07	19.40	18.33	18.07	18.14	–	–	–
GSC2U J133616.1+001733	LP 618- 14	17.97	17.41	17.05	16.29	15.66	14.26	13.74	13.51
GSC2U J133620.4+364829	LP 269- 25	18.87	18.04	17.66	17.51	17.48	–	–	–
GSC2U J134043.4+020348	LHS 2781	19.26	18.11	17.62	17.43	17.36	–	–	–
GSC2U J134107.9+415004	LP 219- 53	18.06	17.67	17.60	17.61	17.69	–	–	–
GSC2U J135118.4+425317	LP 219- 80	17.62	17.05	16.87	16.86	16.93	16.38	15.92	17.23
GSC2U J155611.5+115351	–	–	–	–	–	–	–	–	–
GSC2U J155721.8+141212	LP 504- 10	–	–	–	–	–	–	–	–
GSC2U J162242.0+670112	–	–	–	–	–	–	–	–	–
GSC2U J165237.4−011354	LP 626- 11	–	–	–	–	–	16.19	15.96	17.0
GSC2U J222233.1+122140	–	19.48	17.90	17.30	17.07	16.97	–	–	–
GSC2U J224011.2−030316	LP 700- 65	–	–	–	–	–	16.93	16.56	17.02
GSC2U J231518.5−020942	LHS 3917	–	–	–	–	–	15.49	15.75	14.86
GSC2U J232115.4+010214	LP 642- 52	20.51	19.37	18.84	18.65	18.59	–	–	–
GSC2U J232116.8+010227	LP 642- 53	21.83	19.85	18.94	18.65	18.47	–	–	–
GSC2U J233539.1+123048	–	–	–	–	–	–	–	–	–
GSC2U J233707.4+003240	LP 643- 20	19.34	18.28	17.79	17.61	17.60	16.55	16.17	15.35